Author(s): Miettunen, Kati & Halme, Janne & Vahermaa, Paula & Saukkonen, Tapio & Toivola, Minna & Lund, Peter

Title: Dye Solar Cells on ITO-PET Substrate with TiO[sub 2] Recombination Blocking Layers

Year: 2009

Version: Post print

Please cite the original version:

Miettunen, Kati & Halme, Janne & Vahermaa, Paula & Saukkonen, Tapio & Toivola, Minna & Lund, Peter. 2009. Dye Solar Cells on ITO-PET Substrate with TiO[sub 2] Recombination Blocking Layers. Journal of The Electrochemical Society. Volume 156, Issue 8. B876/1-35. ISSN 0013-4651 (printed). DOI: 10.1149/1.3138129.

Dye Solar Cells on ITO-PET Substrate with TiO_2 Recombination Blocking Layers

Kati Miettunen [a,], Janne Halme [a], Paula Vahermaa [a], Tapio Saukkonen [b], Minna Toivola [a], Peter Lund [a]*

[a] Advanced Energy Systems, Department of Applied Physics, Helsinki University of Technology, P.O. BOX 5100, FIN-02015 TKK, Finland

[b] Engineering Materials Group, Department of Engineering Design and Production, Helsinki University of Technology, P.O. BOX 4200, FIN-02015 TKK, Finland

Abstract

Atomic layer deposited TiO_2 recombination blocking layers were prepared on ITO-PET photoelectrode substrates for dye solar cells and examined using several electrochemical methods. The blocking layers increased the open circuit voltage at low light intensities. At high light intensities decrease of the fill factor due to additional resistance of current transport through the layer was more significant than the positive effect by the reduced recombination. The decrease in the fill factor was reduced by thermal treatment that made the blocking layer more conductive due to a structural change from an amorphous to a crystalline form. Therefore, thinner blocking layers of this type are required for plastic cells prepared at low temperature than for conventional glass dye solar cells made with temperature processing.

Keywords: dye-sensitized, substrate, current leakage, impedance spectroscopy, atomic layer deposition

1. Introduction

Nanostructured dye solar cells (DSC) have traditionally been deposited on glass sheets. Different plastic and metal substrates have been investigated in recent years in order to decrease material costs and advance suitability for roll to roll mass production. Plastic sheets have the advantage of being lightweight and flexible. They can also offer adequate transparency contrary to metals. Flexible dye solar cells are therefore commonly based either solely [1-2] or partly on polymer substrates [3-5]. Several low temperature methods have been presented to prepare both the photoactive and the catalyst layers.

An optimal DSC substrate has high transparency, low sheet resistance, and good stability. It also acts as a physical barrier towards moisture penetration and leakage of the liquid electrolyte and provides mechanical support to the cell structure. An optimal photoelectrode substrate forms a low resistance ohmic contact with the TiO_2 nanoparticle film, but effectively blocks electron transfer to the oxidized species (usually triiodide) in the electrolyte. This so-called recombination from the substrate has predominantly been studied in case of fluorine doped tin oxide (FTO) coated glass substrates [6-13]. Only recently other materials such as stainless steel have been examined [11]. In order to reduce the recombination losses, the use of blocking layers has been introduced [6, 8-10, 13].

It has been detected that recombination losses via the substrate are especially significant at low light intensities [6,7,12]. DSCs on glass are typically designed to be used in building integrated photovoltaic systems in which case they are designed for high light intensities. However, the lightweight plastic solar cells are considered to be suitable for portable applications used typically indoors in low light intensity conditions. Maintaining high open circuit voltage by suppression of the substrate mediated recombination is therefore an essential requirement for plastic DSCs.

Here the electrochemical performance of ITO coated polymer sheet as the photoelectrode substrate is examined in comparison to FTO glass substrates. The effect of atomic layer deposited (ALD) TiO_2 blocking layers is studied as well. In literature the effect of blocking layers on open circuit voltage and fill factor varies considerably [6, 8-10]. Therefore a thorough and critical analysis is motivated to disaggregate the different ways these blocking layers contribute to the photovoltaic performance of the cell. In the analysis several complementary techniques are used: substrate polarization, open circuit voltage decay (OCVD) and electrochemical impedance spectroscopy (EIS). The results from these methods are compared and contrasted with the photovoltaic performance of the solar cells.

2. Experimental Details

2.1 Samples

In this study, we compare two types of solar cells: firstly, the photoelectrode (PE) was prepared by a low temperature compression method [14] and secondly, a conventional PE on FTO-glass substrate was prepared using high temperature sintering of a commercial TiO_2 paste. In addition, solar cells with the low-temperature pressed photoelectrode on FTO-glass were prepared to separate the effect of the substrate from other factors. In addition to the complete solar cells, substrate - counter electrode (SU-CE) cells were made. The substrates of the SU-CE cells were thermally treated and dyed in similar fashion as the PEs to ensure the resemblance to photoelectrode substrate in the solar cell. The solar cell structure was not optimized for maximum efficiency.

The studied substrates were ITO-PET (NV-CT-CH-1S-M-7, 60 Ω/sq, 200 μm, Bekaert Specialty Films, Inc.) and FTO-glass (TEC-15, 15 Ω/sq, 2.5 mm, Pilkington, Hartford Glass Company, Inc.). The substrates were washed with a mild detergent followed by an ultrasonic bath for three minutes first in ethanol and then in acetone. The atomic layer deposition (ALD) of the TiO_2 blocking layers were prepared at 100 °C by Planar Inc. The deposited

film thicknesses were specified to be 4 nm and 35 nm based on ellipsometry using a silicon reference.

Three kinds of photoelectrodes (PE) were made: pressed PEs on both ITO-PET and FTO-glass and sintered PEs solely on FTO-glass. The pressed/low temperature treated photoelectrodes were made by doctor blading a solution of 20 wt% TiO_2 (P25, Degussa) in ethanol, followed by compression at ca. 700 kg/cm^2. The PE was covered with a PTFE foil during the pressing. The ready-made pressed layers were heated at 120 °C before dye sensitization. The sintered/high temperature treated porous TiO_2 layers were deposited by doctor blading a commercial TiO_2 paste (STI) followed by drying at 120 °C and sintering at 450 °C for 30 min. A mask tape (3M Scotch Removable tape, thickness 65 μm) with a hole of 4 mm x 8 mm was employed in distribution of both TiO_2 pastes. TiO_2 layer thickness was typically ca. 15 μm measured with Dektak 6M profiler. The TiO_2 layers were sensitized for 16 h in a N-719 dye solution consisting of 0.32 mM *cis*-bis(isothiocyanato) bis(2,2'-bipyridyl-4,4'-dicarboxylato)-ruthenium(II) bis-tetrabutylammonium (Solaronix) in absolute ethanol.

The counter electrodes were prepared on FTO-glass substrates using thermal deposition from platinum precursor solution consisting of 5 mM $PtCl_4$ (Sigma-Aldrich) dissolved in 2-propanol and heating at 385 °C for 15 min [15]. Typically, the electrolyte contained 0.5 M LiI, 0.03 M I_2 and 0.05 M 4-*tert*-butylpyridine in 3-methoxypropionitrile, and 25 μm thick Surlyn 1702 ionomer resin film spacers were used. Some of the pressed electrodes on ITO-PET were prepared with a thicker layer of TiO_2 (24-30 μm) in which case two spacer foils were used instead of one and the I_2 concentration was increased to 0.05 M to reach the same limiting current.

The electrolyte was inserted through filling holes in the counter electrode which were sealed with a 40 μm thick Surlyn 1601 film and a thin cover glass. Copper tapes served as

current collector contacts. Electrolube conducting silver paint was applied on the interface of the substrate and the tape to reduce resistance.

2.2 Measurements

Photovoltaic measurements were performed using a solar simulator constructed of halogen lamps providing 1000 W/m^2 AM1.5G equivalent light intensity determined by a calibrated silicon reference cell with a spectral filter to mimic typical DSC response. The solar cells were placed on a black surface cooled to 25 °C with Peltier elements. The IV curves were measured using a Keithley 2420 SourceMeter. The ready-made solar cells were provided with black masks with a slightly larger aperture compared to the active area of the cell [16].

The IV-measurements at low light intensities were made with a red LED (λ_{peak} = 639 nm) as the light source. In these measurements as well as in the steady state IV measurements of the SU-CE cells, the data was recorded with Zahner Elektrik's IM6 Potentiostat. The SU-CE cells were measured at the voltage range -0.7 – 0.7 V in 5 mV intervals with 30 s stabilization time for each voltage point. A slow scan rate is required to suppress hysteresis and instability near zero polarization due to double layer charging.

In open circuit voltage decay (OCVD) measurements, the cells were illuminated using the LED light source while keeping the cells at the open circuit. After the V_{OC} had stabilized, the light was turned off and the decay of the open circuit voltage was recorded in 50 ms intervals using an Agilent 34970A data logger. The input impedance of the measurement unit was 10 MΩ and the response time was measured to be less than 40 ms. The OCVD were performed in a black box to avoid stray light.

Electrochemical impedance spectroscopy (EIS) was performed with Zahner Elektrik's IM6 Impedance Measurement unit over the frequency range 100 mHz – 100 kHz in

potentiostatic mode using 10 mV amplitude. The equivalent circuit analysis was made using ZView2 software.

A LI-COR LI-1800 spectroradiometer equipped with an external integrating sphere system was used in the optical measurements in 390-1100 nm wavelength region. To mimic the situation in the solar cells, the samples consisted of a substrate and a thin microscope glass sealed with a 25 μm thick spacer and filled with 3-methoxypropionitrile.

For the analysis of the surface morphology JEOL JSM-7500 scanning electron microscope (SEM) was employed. The x-ray diffraction (XRD) system PANalytical X'Pert PRO MRD was used for analysis of the crystallinity of the blocking layers. For the same purpose we used also Zeiss Ultra 55 field emission scanning electron microscope equipped with Nordlys II digital electron backscatter diffraction (EBSD) detector and HKL Channel 5 software. In the EBSD measurements 10 kV accelerating voltage was employed.

3. Results and Discussion

3.1 Structure of the Blocking Layers

Figure 1 shows the SEM images the TiO_2 blocking layer coated samples on FTO-glass substrate and uncoated FTO-glass substrates. The conductive coating consists of rather large FTO particles (about 100 nm). Since the 4 nm TiO_2 layer is thin compared to the FTO particle size, it is logical that it has only a very slight smoothing effect on the surface image as can be seen when comparing Figures 1a and 1b. The 35 nm coating instead changes the surface features by smoothening the shape of the FTO crystal particles, joining neighbourging small particles together by filling ,and covering the gaps between them (Fig. 1c). In the SEM images we found no changes between the low temperature and high temperature treated blocking layer coated substrates (data not shown).

ALD blocking layers prepared at low temperatures are typically amorphous [17] whereas high temperature treatments make the films crystalline [18]. We therefore expect that the

present ALD TiO_2 layers deposited at 100 °C are amorphous but most likely crystallize during the heat treatment at 450 °C used for the sintering of the nanoporous TiO_2 photoelectrode film on glass. Efforts were made using several techniques to study the crystallinity of the as-prepared and heat-treated ALD films. Crystallinity is typically studied with XRD, but even the 35 nm thick TiO_2 layers were too thin for the measurement system. However, ESBD analysis showed Kikuchi lines corresponding to crystal structures of TiO_2 in the high temperature treated 35 nm TiO_2 film (Fig. 1d) and in the 35 nm thick low temperature treated TiO_2 layer no crystallinity was detected. 4 nm thick layers are too thin for the ESBD measurement, but they are expected to have similar structure as the thicker films.

3.2 Photovoltaic performance

The high temperature treated glass cells produced higher short circuit current density i_{SC} at 1 sun equivalent illumination and thus also higher efficiency compared to the low temperature treated ITO-PET cells (Fig. 2 and Table 1). The positive effect of the high temperature treatment of the porous TiO_2 film on the cell performance is well known, and is attributed to the light sintering of the particle film yielding improved physical and electrical contact between the TiO_2 nanoparticles. In the low temperature treated, pressed TiO_2 films the electron diffusion length is shorter than the film thickness and thus not all injected electrons are collected which leads to a lower i_{SC} as seen in Figure 2 and Table 1. This deduction is supported by the EIS data discussed later.

In 1 sun equivalent illumination the typical positive impact brought by the blocking layers on the photovoltaic characteristics is the slight increase of V_{OC} (Fig. 2 and Table 1). i_{SC} remained about the same in the application of the 4 nm blocking layers whereas with the 35 nm layers it decreased. Except for the low temperature treated cells with the 35 nm layer, these differences in i_{SC} correspond to decrease in the transmittance of the PE substrate: 4 nm

TiO_2 layer decreased the transmittance less than 1 % and the 35 nm layer about 5 % in the visible region both ITO-PET and FTO-glass (data not shown).

The blocking layers on ITO-PET decreased the fill factor clearly whereas on FTO the decrease was very small. The influence of the blocking layers on the IV curve of the ITO-PET cells is similar to what would be expected from a decreased shunt resistance, although this cannot be the actual reason. Considering the two components that contribute the shunt resistance in the cell, namely the porous TiO_2/electrolyte interface and the substrate/electrolyte interface, the former was similar in all the cells made with the same thermal processing, while the latter only increased when a blocking layer was applied as indicated by the substrate polarization and EIS measurements discussed later.

The IV curves were similar in both low and high temperature treated FTO-glass cells with the 4 nm blocking layer (data not shown). Contrary to this, low temperature treated FTO-glass cells with the 35 nm blocking layer (data not shown) showed as poor performance as the ones on ITO-PET with the 35 nm blocking layer. Therefore, the performance loss with the 35 nm layer can be attributed to the low temperature treatment unlike with the 4 nm blocking layer.

The blocking layer is, however, clearly required to reach high voltage at low light intensities since V_{OC} was increased clearly due to the application of the 4 nm TiO_2 blocking layers in both ITO-PET and FTO-glass cells (Fig. 3). Increasing the blocking layer thickness to 35 nm had no impact on the intensity dependence of the V_{OC} in the high temperature treated glass cells. The fact that the influence of the blocking layers on V_{OC} becomes more significant towards lower light intensities is in good correspondence with literature [6-7,12] and has been linked with substrate mediated recombination.

The linearity of V_{OC} versus $\log(i_{SC})$ with a slope of 110 mV/decade in the blocking layer coated cells (Fig. 3) is indicative of non-ideal diode-like recombination characteristics of the

photoelectrode, the non-ideality factor being ca. 1.8-1.9 in this case. Non-ideal diode characteristics of the DSC have been attributed to recombination via the substrate or surface states in the nanoporous TiO_2 film [19]. As shown later, the recombination via substrate should be suppressed by the blocking layers, which implies that the non-ideality is likely related to recombination via the surface states in this case.

3.3 Polarization of the substrate

Substrate polarization measurements are frequently used for measuring the current leakage from the photoelectrode substrate and for verifying the satisfactory performance of the blocking layer. Figure 4 indicates that the recombination current from both ITO-PET and high temperature treated FTO-glass substrates were equal. The small effect of the blocking layers at 1 sun illumination can be explained with substrate polarization data: the comparison of the typical DSC i_{SC} (10-20 mA/cm^2) with the recombination current from the bare substrate shows a difference of several orders of magnitude that suggests that both ITO-PET and FTO-glass are as such sufficiently inactive towards triiodide reduction reaction at high light intensities.

All the tested blocking layers suppressed the current by about one decade throughout the studied voltage range compared to the bare substrate except for the 35 nm layer on ITO-PET which decreased it even more. This is due to the low temperature treatment: low temperature treated FTO-glass cells with the 35 nm layer (data not shown) presented as low currents as the ITO-PET cells with the 35 nm layer.

Compared to the previous results in the literature [7-9,13], the data in Figure 4 demonstrates excellent recombination blocking characteristics: for the heat-treated FTO-glass substrates the recombination currents here were one to two decades smaller, and for the substrates with blocking layer similar or lower than reported previously.

3.4 Open circuit voltage decay

Open-circuit voltage decay (OCVD) is an efficient technique for quantitative study of electron transfer at the photoelectrode. In the OCVD the gradual loss of photogenerated electrons due to recombination is monitored by measuring the transient decay of the cell voltage after switching off the light. Since the cell is kept at open circuit during the experiment, the data is not obscured by the transient response by other cell components and the measured voltage can be assigned solely to the photoelectrode. From the transient data, the effective electron lifetime τ_{eff} is obtained as [20]:

$$t_{eff} = -\frac{k_B T}{e}\left(\frac{dV_{OC}}{dt}\right)^{-1} \quad (1)$$

where k_B is the Boltzmann coefficient, T the temperature, e the elementary charge, and t the time. Note, that the OCVD data of the blocking layer coated solar cells in Figure 5 should be interpreted qualitatively for voltages less negative than -0.2 V where the input impedance of the measurement device may not be significantly larger than the charge transfer resistance of the photoelectrode/electrolyte interface (Fig. 10).

The blocking layers increased the electron lifetime primarily at the small negative voltage as shown in Figure 5. This result is in good accordance with literature [21,22]. According to literature [21,22], the electron lifetimes at large negative voltages correspond to the porous TiO_2 layer and they should be similar for similarly prepared films. This was seen with both low temperature (Fig. 5) and high temperature treated FTO-glass cells. Interestingly, the application of the 4 nm blocking layer on the ITO-PET caused an increase in τ_{eff} also at the large negative voltages.

The low temperature treated cells with the 35 nm layer gave high electron lifetimes. These cells illustrated also a very low current in the substrate polarization measurements. The photovoltaic performance of these cells was, however, very poor. This demonstrates the fact

that while OCVD and polarization measurements are useful to clarify interfacial charge transfer in DSC, they do not provide all necessary information to explain the photovoltaic cell performance. For this, also techniques sensitive to the charge transport in the cell are needed. Electrochemical impedance spectroscopy (EIS) is one of the most effective techniques for this purpose.

3.5 EIS response and equivalent circuit fitting

Sintering of the photoelectrode layer has a significant effect on the EIS response of the cell because it decreases the transport resistance in the TiO_2 film notably. Hence, to see the effect of the substrate instead of the temperature treatment, we discuss primarily the data of the low temperature treated cells in the EIS analysis. A separate remark is made if the data is from the high temperature treated cells.

The general equivalent circuit of a DSC similar to the one presented by Fabregat-Santiago et al. [23] is illustrated in Figure 6. Constant phase elements (CPE) are used instead of pure capacitors as they describe better the uneven and porous electrodes. The circuit in Figure 6 can be approximated with simplified circuits depending on the voltage [21]. From -0.1 V to -0.3 V only one semicircle corresponding to the photoelectrode could be detected in the low frequencies and in the data fitting equivalent circuit (a) (Fig. 7) was employed. From -0.4 V to -0.7 V, the photoelectrode showed a Gerischer type response [21] and there was at least one semicircle detectable at the higher frequencies (Fig. 8). For the data fitting of this data, equivalent circuit (b) (Fig. 7) was used. In the case of Gerischer type response only the upper limit for R_{CT} can be estimated as explained in appendix. For SU-CE cells there was one semi-circle present throughout the studied voltage range and equivalent circuit (a) was used.

The blocking layer brings along additional R/CPE components which may contribute to the EIS response. Indeed, the presence of at least one such component was detected as

shown later. In the most general case, the impedance of the blocking layer coated substrates can be considered to consist of three series connected R/CPE couples between the conductive coating of the substrate (TCO) and the porous TiO_2 film: the substrate/compact TiO_2 interface $R_{TCO/BL}$, the compact TiO_2 bulk layer R_{BL}, and the compact TiO_2/porous TiO_2 interface $R_{BL/TiO2}$. In the case of the blocking layer coated samples we denote the sum of these resistances with R_{CO}, whereas R_{SU} consists of the series connection of the substrate/compact TiO_2 interface, the compact TiO_2 bulk layer, and the compact TiO_2/electrolyte interface $R_{BL/EL}$:

$$R_{CO} = R_{TCO/BL} + R_{BL} + R_{BL/TIO2} \quad (2)$$

$$R_{SU} = R_{TCO/BL} + R_{BL} + R_{BL/EL} \quad (3)$$

Typically, a conducting homogenous bulk layer functions as a simple resistor without a capacitive component. However, a thin compact TiO_2 blocking layer can be alternatively regarded as an insulator between two conductive layers and hence its impedance could be equivalent to a leaking parallel plate capacitor. The capacitance of the blocking layer C_{BL} can be estimated then as:

$$C_{BL} = e_r e_0 \frac{A}{d_{BL}} \quad (4)$$

where ε_r is the relative permittivity of the blocking layer material, ε_0 the vacuum permittivity, A the area of the layer, and d_{BL} the thickness of the layer.

According to the EIS measurements, the presence of a blocking layer had only a very slight impact on the ohmic resistance R_s of the cell. It can be concluded that the ALD coating did not have a marked impact on the sheet resistance of the conducting oxide coating of the substrates.

3.6 High frequency EIS response

The high frequency semicircle on the left in Figure 8a is usually attributed to charge transfer at the counter electrode R_{CE}. Differences between different cell types could be seen although the counter electrodes should have shown equal performance due to similar preparation. Quantitative comparison of individual impedance elements between different cells is complicated by the fact that the voltage over a single electrode is not readily accessible by the standard two electrode measurements. Accurate comparison of the single electrode performance is, however, easily achieved if the data is analyzed as a function of external current as described in our previous work [11].

R_{HF} of the glass solar cells equaled with R_{CE} measured in symmetric CE-CE cells (data not shown). It can therefore be concluded that in the case of the glass cells the high frequency response is governed by the charge transfer at the counter electrode in case of FTO-glass substrates. However, Figure 9 shows that R_{HF} of the ITO-PET cells is much higher compared to those of the FTO-glass cells. When R_{CE} is subtracted from the R_{HF}, a significant impedance component remains. The dependence of R_{HF} on the photoelectrode substrate suggests that the component is caused by R_{CO}. Similar increase in the R_{HF} has been detected in a smaller scale also previously when using different substrates [24].

The presence of the 4 nm layer on ITO-PET increased R_{HF} even further. In the case of the low temperature treated cells with the 35 nm layer, there was only a single large semi-circle which was at least an order of magnitude larger than the total resistance of the uncoated cells at the corresponding voltages (data not shown). Since both the counter electrodes and the porous TiO_2 layers in the cells should be similar with and without a blocking layer, the presence of a very large semicircle suggests that the R_{CO} is dominating the response and is overlapping not only with R_{CE} but also with R_{CT} in those cells.

For the glass cells R_{CE} was of the same magnitude as R_s and Z_d (data not shown) which together form the resistance which decreases the fill factor in the photovoltaic measurements. R_{CO} values measured here for ITO-PET cells are larger than R_{CE} and therefore they are expected to have observable impact on the slope of the IV-curve near open-circuit state and also on the fill factor. The R_{CO} of the 35 nm layer ITO-PET cells is in fact so large that it is expected to flatten the IV curve to the extent that it lowers i_{SC} significantly. In agreement with this, the IV-curves of the ITO-PET cells without blocking layer have steeper slope compared to the ones with the blocking layers and suppressed i_{SC} in case of the 35 nm layer (Fig. 2 and Table 1). Note, that the R_{CO} was voltage dependent which causes the IV curve of the low temperature treated 35 nm coated solar cells to deviate from a straight line. In the case of the low temperature treated SU-CE cells with the 35 nm layer, it is likely that R_{CO} had a marked contribution to the low current seen in the polarization measurements (Fig. 4). In case of other substrate/blocking layer combinations, the other resistances were significantly smaller than those of the blocking layer/electrolyte interface and the lowering of the leakage current in Figure 4 can be attributed to actual decrease in electron recombination.

As mentioned above, the blocking layers produce three possible EIS components that can be linked with the increased R_{CO}. If the bulk resistance of the compact blocking layer were to contribute to the high frequency impedance arc corresponding to R_{CO}, the dielectric capacitance of the blocking layer (eq. 4) would have to be of the same order of magnitude as the measured capacitance C_{CO}. Using the relative permittivity of TiO_2 varying from 25 to 100, which is a larger range than typically observed for TiO_2 thin films [17,25], the dielectric capacitance of the 4 nm blocking layer was calculated to range from $2 \cdot 10^{-6}$ F to $7 \cdot 10^{-6}$ F. The measured value for cells with the 4 nm blocking layer on ITO-PET was approximately $2 \cdot 10^{-5}$ F. Since the C_{CO} values do not correspond and since the material difference between

the compact TiO_2/porous TiO_2 should not be significant, the increased R_{CO} is most likely due to the resistance at the ITO/compact TiO_2 interface in the case of the ITO-PET cells with the 4 nm layer. In the case of the low temperature treated cells with the 35 nm blocking layer, the measured capacitance varied from $7 \cdot 10^{-7}$ F to $2 \cdot 10^{-6}$ F which partly matches with the calculated C_{BL} values which range from $2 \cdot 10^{-7}$ F to $8 \cdot 10^{-7}$ F. Hence, for the low temperature treated 35 nm films a contribution from bulk resistance of the blocking layer on the measured R_{HF} cannot be ruled out.

It would be logical that the thickening of the blocking layer would increase the bulk resistance. The effect does not, however, appear in the high temperature treated cells. The high temperature treatment apparently induced a structural change of the TiO_2 blocking layers from amorphous to crystalline as already mentioned. The change from amorphous to crystalline improves the conductivity of the film by introducing oxygen vacancies and by formation of grain boundaries which act as efficient current pathways [17]. Amorphous TiO_2 films are therefore expected to be less conductive than crystalline ones. As a result, the amorphous 35 nm TiO_2 layer appears to have been too thick whereas the amorphous 4 nm layer was thin enough to function as blocking layer in DSCs, whereas in the case of the crystalline TiO_2 layer obtained by the heat treatment even the 35 nm thick layers were thin enough to provide sufficiently low resistance. Based on the literature, it is known that even the crystalline compact TiO_2 layers become too resistive when the film thickness exceeds approximately 200 nm [9]. It appears that thicker ALD layers can be used in the high temperature treated cells than in the low temperature cells.

3.7 Photoelectrode EIS response

The resistance connected to the low frequency EIS response (R_{LF}) for solar cells and SU-CE cells prepared using low temperature treatment is displayed in Figure 10. It was estimated that in Figure 10 the external cell voltage differs from the voltage over the PE only

in the presence of the porous TiO_2 layer at voltages more negative than -0.4 V and at most by some tens of millivolts. Hence, the voltage corrections such as employed in [11] were omitted here as they would not have resulted in any changes in the main conclusions. The 35 nm blocking layer coated cells are omitted here as they were already discussed above.

The presence of the 4 nm thick blocking layer increased the recombination resistance of the SU-CE cells approximately 1 to 2 orders of magnitude. This result is equivalent with the substrate polarization measurements as to be expected since the EIS results show the derivative of the polarization curve. In the case of complete solar cells, the 4 nm blocking layer increased the recombination resistance significantly at small negative potentials (Fig. 10). This result is in good correspondence with the OCVD data and the low light intensity measurements which both showed improved performance at small negative potentials. The OCVD data and the EIS data are also linked since the effective electron lifetime τ_{eff} (Fig. 5) is the product of corresponding resistance (Fig. 10) and capacitance [26].

At the high negative potentials a transmission line feature characteristic for a porous electrode film could be detected. At that voltage region, the EIS response corresponds to the recombination from the porous TiO_2 layer and, since the layers should be similar in all the cells in Figure 10, their similar performance is an expected result. As the recombination resistance of the 4 nm blocking layer coated increased substantially the substrates' recombination resistance (Fig. 10), the recombination current flows through the porous TiO_2 also at the smaller voltages in those cells.

The recombination resistance of the uncoated solar cells showed repeatably approximately one order of magnitude smaller values compared to the SU-CE cells, the performance of which should correspond to that of the photoelectrode substrate. This observation contradicts the result of Fabregat-Santiago et al., who found that the photoelectrode resistance of a solar cell equaled the recombination resistance of the substrate at small

negative voltages [21]. Finally, we point out that the data in Figure 10 cannot be explained with a simple parallel connection of the porous TiO_2 layer with the substrate (Fig. 6) even when taking into account the effect of substrate/TiO_2 interface in the small negative voltages. This suggests that there might be some kind of interaction between the substrate and the TiO_2 layer which the EIS model cannot explain because it considers the components to be independent.

4. Conclusions

Low temperature ALD TiO_2 blocking layers were applied on ITO-PET photoelectrode substrates and their electrochemical performance was examined using multiple complementary techniques. The recombination from the ITO-PET substrate is on a similar level than that from the FTO-glass substrates. At high light intensities, both ITO-PET and FTO-glass were sufficiently resistant towards recombination even without blocking layers. The blocking layers proved to be useful, however, in gaining high open circuit voltage at low light intensities.

The other resistance components introduced by the blocking layer in addition to the recombination resistance were shown to be important: In the case of the ITO-PET cells with 4 nm blocking layer, a high frequency impedance component was found in the EIS and attributed to the contact resistance between the ITO and the compact TiO_2. In the low temperature treated cells with the 35 nm layer an even larger resistance was detected and it appeared to be dominated by the bulk resistance of the TiO_2 blocking layer.

As the difference between high and low temperature treated 35 nm layers showed, temperature treatments have a profound effect on the performance of the blocking layer. The effect was linked with improved conductivity due a structural change from amorphous to crystalline in the heat treatment. In practice, this suggests that in the case of this type of a film thicker layers can be employed in high temperature treated cells whereas low

temperature treated cells require thinner ones. Hence, the blocking layers need to be separately optimized for low temperature treated DSCs by minimization of fill factor losses due to resistivity of the blocking layer while maintaining low recombination resistance.

Acknowledgement

The support of Finnish Funding Agency for Technology and Innovation (Tekes) is acknowledged. K. M. is grateful for the scholarship of the Graduate School of Energy Technology. We thank Planar Systems, Inc (Nora Isomäki, currently Beneq Oy, nora.isomaki@beneq.com) for the ALD blocking layers. We also thank Juuso Korhonen (Department of Applied Physics, TKK) for the SEM images and Pasi Kostamo (Department of Micro and Nanosciences, TKK) for the XRD measurements. This work made use of Helsinki University of Technology, Nanomicroscopy Center (TKK-NMC) Facilities.

Appendix A

Interpretation of the Gerischer type impedance response

The low frequency end of the Gerischer response is a semi-circle while the high frequency end displays a 45° slope in the complex plane. The Gerischer response corresponds to a situation where the electron transport resistance is equal or higher than the recombination resistance of the photoelectrode film, and thus the electron diffusion length L is smaller than the film thickness d. In such a case, R_{CT} and R_t cannot be determined independently by equivalent circuit fitting, since in this case the transmission line model reduces to the Gerischer impedance that is characterized by only one independent resistance parameter, the Gerischer resistance $R_G = (R_{CT}R_t)^{1/2}$, which corresponds to the total width of the impedance arc [21]. However, using the additional information that Gerischer response is observed only when $R_{CT} < R_t$ (approximately), the upper limit $R_{CT,max}$ and the lower limit $R_{t,min}$ can be determined: fitting a semicircle to the low frequency end of the spectrum yields an estimate

for $R_{CT,max}$. Any larger R_{CT} value than this, that is also consistent with the total width of the impedance arc, would not result in a Gerischer impedance but an R_t slope and a R_{CT} semi-circle would be separated in the EIS spectrum, as described by the transmission line impedance model.

References

[1] H. Lindström, A. Holmberg, E. Magnusson, S. Lindquist, S. Malmqvist, A. Hagfeldt, Nanoletters 1 (2001) 97-100.

[2] T. Miyasaka, M. Ikegami, Y. Kijitori, J. Electrochem. Soc. 154 (2007) A455-A461.

[3] M.G. Kang, N.-G. Park, K.S. Ryu, S.H. Chang, K.-J. Kim, Sol. Energy Mater. Sol. Cells 90 (2006) 574-581.

[4] S. Ito, N-L. C. Ha, G. Rothenberger, P. Liska, P. Comte, S.M. Zakeeruddin, P. Péchy, M.K. Nazeeruddin, M. Grätzel, Chem. Commun. 38 (2006) 4004–4006.

[5] Y. Jun, J. Kim, M.G. Kang, Sol. Energy Mater. Sol. Cells 91(2007) 779-784.

[6] S. Hore, R. Kern, Appl. Phys. Lett. 87 (2005) 2635504.

[7] P.J. Cameron, L.M. Peter, S. Hore, J. Phys. Chem. B 109 (2005) 930-936.

[8] J. Xia, N. Masaki, K. Jiang, S. Yanagida, J. Phys. Chem. B 110 (2006) 25222-25228.

[9] J. Xia, N. Masaki, K. Jiang, S. Yanagida, J. Phys. Chem. C 111 (2007) 8092-8097.

[10] R. Hattori, H. Goto, Thin Solid Films 515 (2007) 8045-8049.

[11] K. Miettunen, J. Halme, M. Toivola, P. Lund, J. Phys. Chem. C 112 (2008) 4011-4017.

[12] A. Burke, S. Ito, H. Snaith, U. Bach, J. Kwiatkowski, M. Grätzel, Nano Lett. 4 (2008) 977-981.

[13] P.J. Cameron, L.M. Peter, J. Phys. Chem. B 107 (2003) 14394-14400.

[14] H. Lindström, E. Magnusson, A. Holmberg, S. Södergren, S. Lindquist, A. Hagfeldt, Sol. Energy Mater. Sol. Cells 73 (2002) 91-101.

[15] N. Papageorgiou, W.F. Maier, M. Grätzel, J. Electrochem. Soc. 144 (1997) 876-884.

[16] S. Ito, K. Nazeeruddin, P. Liska, P. Comte, R. Charvet, P. Péchy, M. Jirousek, A. Kay, S. Zakeeruddin, M. Grätzel, Prog. Photovolt: Res. Appl. 14 (2006) 581-601.

[17] G. D. Wilk, R. M. Wallace, J. M. Anthony, J. Appl. Phys. 89 (2001) 5243-5275

[18] J. Aarik, A. Aidla, A.-A. Kiisler, T. Uustare, V. Sammelselg, Thin Solid Films 305 (1997) 270-273.

[19] L. M. Peter, J. Phys. Chem. C 2007, 111, 6601-6612.

[20] A. Zaban, M. Greenshtein, J. Bisquert, ChemPhysChem 4 (2003) 859-864.

[21] F. Fabregat-Santiago, J. Bisquert, G. Garcia-Belmonte, G. Boschloo, A. Hagfeldt, Sol. Energy Mater. Sol. Cells 87 (2005) 117-131.

[22] P.J. Cameron, L.M. Peter, J. Phys. Chem. B 109 (2005) 7392-7398.

[23] F. Fabregat-Santiago, J. Bisquert, E. Palomares, L. Otero, D. Kuang, S.M. Zakeeruddin, M. Grätzel, J. Phys. Chem. C 111 (2007) 6550 -6560.

[24] T. Hoshikawa, M. Yamada, R. Kikuchi, K. Eguchi, J. Electrochem. Soc. 152 (2005) E68-E73.

[25] S. Duenãs, H. Castán, H. Garciá, E. San Andrés, M. Toledano-Luque, I. Mártil, G. Gonzáles-Díaz, K. Kukli, T. Uustare, J. Aarik, Semicond. Sci. Technol. 20 (2005) 1044-1051.

[26] J. Bisquert, G. Garcia-Belmonte, F. Fabregat-Santiago, N. S. Ferriols, P. Bogdanoff, E.C. Pereira, J. Phys Chem. B, 104 (2000) 2287-2298.

Figure captions

Figure 1. Typical SEM-images of a) uncoated FTO glass, b) FTO glass with 4 nm TiO_2 layer, and c) FTO glass with 35 nm TiO_2 layer without temperature treatments. d) EBSD image of the high temperature treated 35 nm TiO_2 blocking layer on plain glass showing Kikuchi lines.

Figure 2. Typical current-voltage curves of the low temperature treated ITO-PET and high temperature treated FTO-glass cells with and without a blocking layer of different thickness.

Figure 3. Open circuit voltage (V_{OC}) of the low temperature (LT) treated ITO-PET cells and the high temperature (HT) treated glass cells with and without the TiO_2 blocking layers as a function of short circuit current density (i_{SC}).

Figure 4. Polarization curves of a) the bare and the compact TiO_2 coated ITO-PET and b) FTO-glass substrates in the dark. The ITO-PET substrates were treated at low temperature (LT) and FTO-glass at high temperature (HT). The error bars indicate standard deviation.

Figure 5. Typical effective electron lifetime of low temperature (LT) treated solar cells deposited on a) ITO-PET and b) high temperature (HT) treated FTO-glass with and without a compact TiO_2 layer.

Figure 6. General equivalent circuit model of a DSC similar to the one presented by Fabregat-Santiago et al. [23]. R_s is the ohmic series resistance caused by sheet resistance of the substrates, current collector contacts etc. CPE_{SU} and R_{SU} are the CPE and charge

transfer resistance at the PE substrate/electrolyte interface. CPE_{CO} and R_{CO} are the CPE and charge transfer resistance between the PE substrate and the porous TiO_2. R_t (= $r_t d$) is the electron transport resistance and d is the thickness of the layer. CPE_{CT} (= cpe_{CT}/d) and R_{CT} (= r_{CT}/d) are the CPE and the charge transfer resistance at the TiO_2/electrolyte interface. Z_d is the mass transfer impedance at the counter electrode due to ionic diffusion in the electrolyte. CPE_{CE} and R_{CE} are the CPE and charge transfer resistance at the counter electrode/electrolyte interface.

Figure 7. Equivalent circuits used in the data fitting a) in the case where transport resistance in the TiO_2 could be omitted and b) in the case where it could be included. CPE_{LF} and R_{LF} mark for the EIS component detected in low frequencies which depending on the voltage can be linked with different photoelectrode/electrolyte interfaces and/or photoelectrode components. CPE_{HF} and R_{HF} correspond to the charge transfer components observed at high frequencies which, in practice, are CPE_{CE} and R_{CE} and/or CPE_{CO} and R_{CO}.

Figure 8. Example EIS data of DSCs with low temperature treated photoelectrodes at -0.6 V in the dark. a) Imaginary impedance versus real impedance. b) Imaginary impedance versus frequency. The markers refer to the measured data and the continuous lines to the fitted data.

Figure 9. Resistance of the high frequency impedance component R_{HF} of the low temperature treated solar cells with and without blocking layer in comparison to that of the cells with high temperature treated (HT) photoelectrode on FTO-glass.

Figure 10. Typical solar cell and SU-CE cell and substrate resistances of low temperature treated a) ITO-PET and b) FTO-glass cells. In case of the samples which contain porous TiO_2, only the upper limit of R_{LF} could be determined at the voltages more negative than -0.4 V due to the Gerischer type response.

Table 1. Performance characteristics and their standard deviations for the low temperature treated ITO-PET and high temperature treated FTO-glass cells with and without TiO_2 blocking layers of different thicknesses.

substrate and blocking layer thickness (nm)	number of cells	V_{OC} (mV)	i_{SC} (mA cm^{-2})	*FF* (%)	η (%)
ITO-PET					
0	4	636 ± 9	8.2 ± 0.4	54 ± 1	2.8 ± 0.1
4	4	651 ± 9	8.1 ± 0.6	44 ± 2	2.3 ± 0.1
35	3	510 ± 70	0.03 ± 0.02	41 ± 4	0.006 ± 0.004
FTO-Glass					
0	7	642 ± 9	13.8 ± 0.2	52 ± 3	4.6 ± 0.3
4	4	658 ± 14	13.6 ± 0.1	51 ± 1	4.6 ± 0.2
35	4	647 ± 25	13.0 ± 0.6	48 ± 4	4.0 ± 0.2

Figure 1.

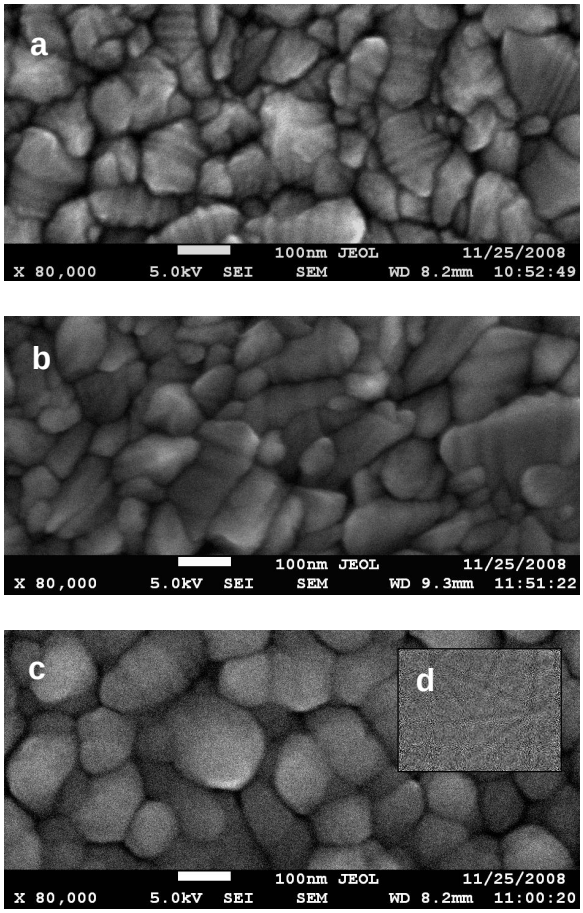
a
100nm JEOL
11/25/2008
X 80,000 5.0kV SEI SEM WD 8.2mm 10:52:49
b
100nm JEOL
11/25/2008
X 80,000 5.0kV SEI SEM WD 9.3mm 11:51:22
c
d
100nm JEOL
11/25/2008
X 80,000 5.0kV SEI SEM WD 8.2mm 11:00:20

Figure 2.

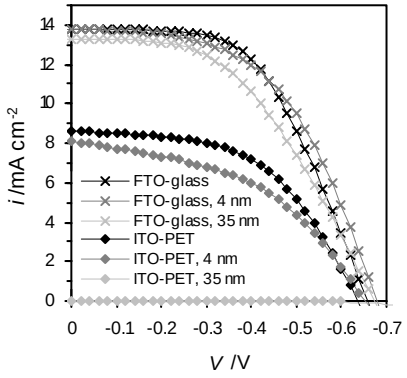
14
12
10
8
6
4
2
0
i /mA cm-2
FTO-glass
FTO-glass, 4 nm
FTO-glass, 35 nm
ITO-PET
ITO-PET, 4 nm
ITO-PET, 35 nm
0
-0.1
-0.2
-0.3
-0.4
-0.5
-0.6
-0.7
V /V

Figure 3.

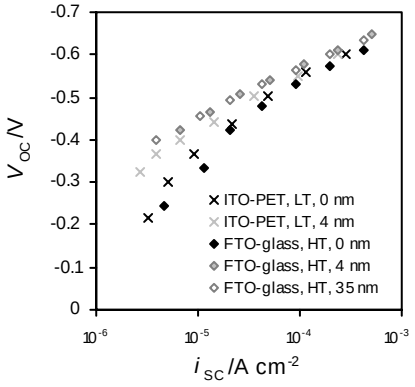
-0.7
-0.6
-0.5
-0.4
-0.3
-0.2
-0.1
0
V_{OC}/V
10^{-6}
10^{-5}
10^{-4}
10^{-3}
i_{SC}/A cm^{-2}
ITO-PET, LT, 0 nm
ITO-PET, LT, 4 nm
FTO-glass, HT, 0 nm
FTO-glass, HT, 4 nm
FTO-glass, HT, 35 nm

Figure 4.

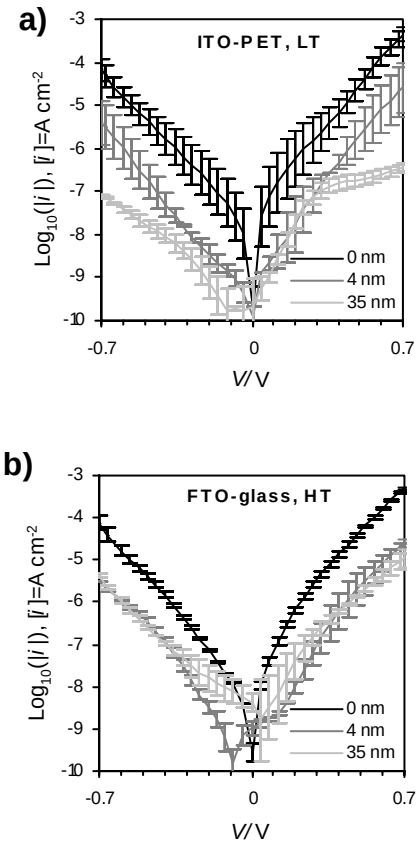
a)
ITO-PET, LT
Log10(|j|), [j]=A cm-2
-3
-4
-5
-6
-7
-8
-9
-10
-0.7
0
0.7
V/ V
0 nm
4 nm
35 nm
b)
FTO-glass, HT
Log10(|j|), [j]=A cm-2
-3
-4
-5
-6
-7
-8
-9
-10
-0.7
0
0.7
V/ V
0 nm
4 nm
35 nm

Figure 5.

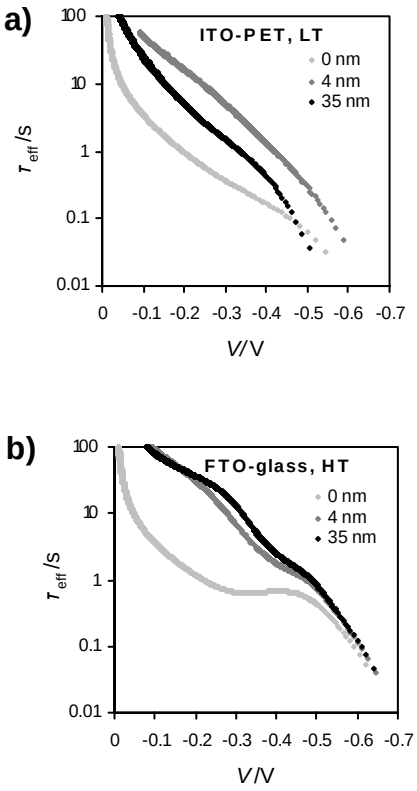
a)
ITO-PET, LT
0 nm
4 nm
35 nm
100
10
1
0.1
0.01
τ_{eff}/s
0
-0.1
-0.2
-0.3
-0.4
-0.5
-0.6
-0.7
V/V
b)
FTO-glass, HT
0 nm
4 nm
35 nm
100
10
1
0.1
0.01
τ_{eff}/s
0
-0.1
-0.2
-0.3
-0.4
-0.5
-0.6
-0.7
V/V

Figure 6.

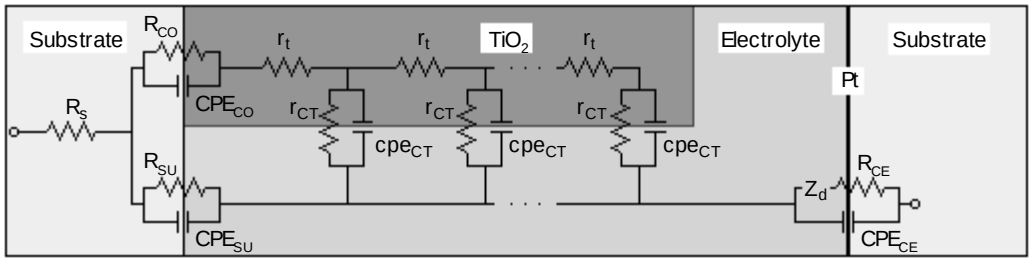
Substrate
R_{CO}
r_t
r_t
TiO_2
r_t
Electrolyte
Substrate
Pt
R_s
CPE_{CO}
r_{CT}
r_{CT}
r_{CT}
cpe_{CT}
cpe_{CT}
cpe_{CT}
R_{SU}
Z_d
R_{CE}
CPE_{SU}
CPE_{CE}

Figure 7.

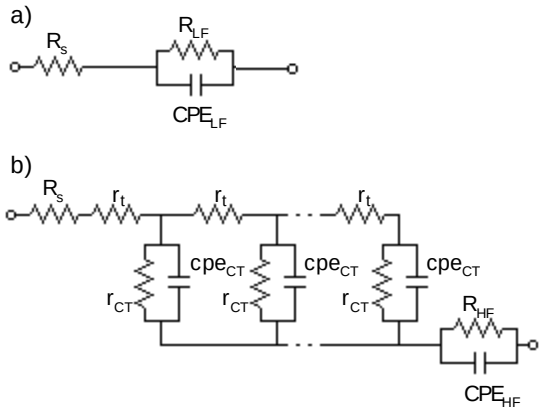
a)
R_s
R_{LF}
CPE_{LF}
b)
R_s
r_t
r_t
r_t
cpe_{CT}
cpe_{CT}
cpe_{CT}
r_{CT}
r_{CT}
r_{CT}
R_{HF}
CPE_{HF}

Figure 8.

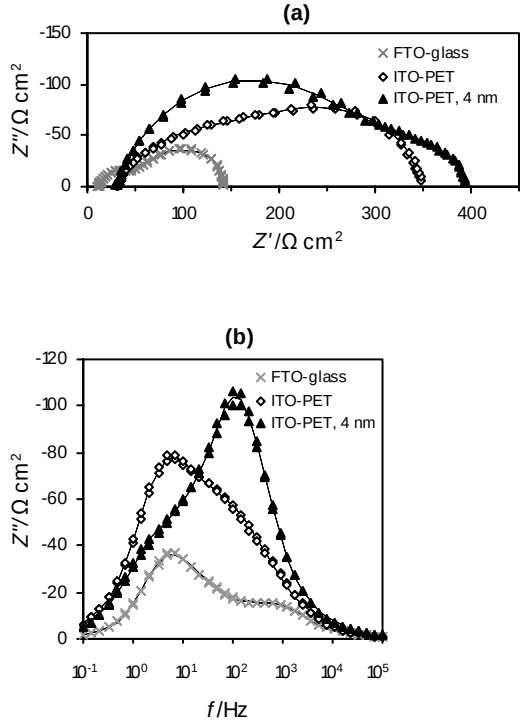
(a)
FTO-glass
ITO-PET
ITO-PET, 4 nm
Z''/Ω cm²
Z'/Ω cm²
(b)
FTO-glass
ITO-PET
ITO-PET, 4 nm
Z''/Ω cm²
f/Hz

Figure 9.

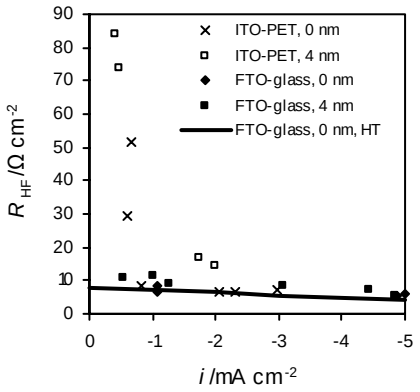
ITO-PET, 0 nm
ITO-PET, 4 nm
FTO-glass, 0 nm
FTO-glass, 4 nm
FTO-glass, 0 nm, HT
R_{HF} /Ω cm^{-2}
i /mA cm^{-2}
90
80
70
60
50
40
30
20
10
0
0
-1
-2
-3
-4
-5

Figure 10.

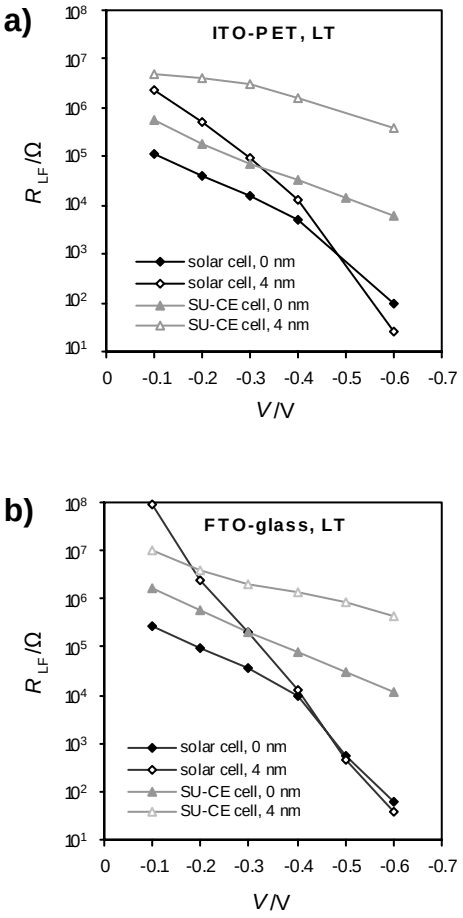
a)
ITO-PET, LT
R_{LF}/Ω
10^8
10^7
10^6
10^5
10^4
10^3
10^2
10^1
solar cell, 0 nm
solar cell, 4 nm
SU-CE cell, 0 nm
SU-CE cell, 4 nm
0
-0.1
-0.2
-0.3
-0.4
-0.5
-0.6
-0.7
V/V
b)
FTO-glass, LT
R_{LF}/Ω
10^8
10^7
10^6
10^5
10^4
10^3
10^2
10^1
solar cell, 0 nm
solar cell, 4 nm
SU-CE cell, 0 nm
SU-CE cell, 4 nm
0
-0.1
-0.2
-0.3
-0.4
-0.5
-0.6
-0.7
V/V